Research Article

Numerical Simulation of Mixed-Mode Fatigue Crack Growth for Compact Tension Shear Specimen

Yahya Ali Fageehi [ID] **and Abdulnaser M. Alshoaibi** [ID]

Department of Mechanical Engineering, Jazan University, P. O. Box 706, Jazan 45142, Saudi Arabia

Correspondence should be addressed to Abdulnaser M. Alshoaibi; alshoaibi@gmail.com

This work concentrates on the fracture behaviour of the compact tension specimen under mixed-mode loading, and numerical investigation using ANSYS Mechanical APDL 19.2 finite element program with different modes of mix angles is carried out. The prediction of mixed-mode fatigue life under constant amplitude fatigue loading for the compact tension shear specimen (CTS) is employed using Paris' law model for two different loading angles with agreement to the experimental results. The predicted values of ΔK_{eq} were compared with the experimental and analytical data for various models. Depending on the analysis, the findings of the present study show consistency with the results achieved with similar models of predicting the equivalent stress intensity factor. In addition, the direction of crack growth derived from the analysis was observed to follow the same trend of the literature experimental results.

1. Introduction

This work describes the use of ANSYS Mechanical APDL 19.2 finite element program in crack analysis of the engineering structures containing discontinuities and holes. In the proposed study of the cracks throughout elastic materials, linear elastic fracture mechanics are employed where the crack driving force called stress intensity factor (SIF) is used as a measure of fracture associated with the materials threshold SIFs (K_{th}) for dynamic loading. The accuracy of a crack propagation simulation depends highly on the accuracy achieved for the calculated SIFs. Engineering structures are generally used under periodic and cyclic loading conditions [1] [2–7] [6]. The periodic as well as cyclic loading decreases the load limit required to initiate deformation in the material under static loading and results in progressive fracture leading to catastrophic failures of the material known as fatigue failures [6]. It has been estimated that 60% to 80% of the failures of mechanical components are associated with fatigue [8]. Various problems concerning fatigue crack growth can be found in the literature using different approaches for simple and complex geometries in two and three dimensions [9–13]. Combined action of tensile stress, cyclic stress, and plastic strain initiates failure due to fatigue phenomena. If any of these three does not exist, it will not trigger and spread a fatigue crack growth [14]. As environmental loads are also multidirectional in nature, the fatigue cracks may propagate under mixed-mode conditions [15–18]. The majority of failures in service is of mixed-mode type, where the cracks do not propagate in the direction normal to the applied load. However, the majority of fatigue crack growth behavior studies focus on mode I cracks, whereas the cracks and defects in actual engineering components (e.g., pressure vessels, pipelines, and fan blades) tend to be plane-stress mixed-modes I–II cracks [19]. In reality also mixed mode can be observed, for example, in turbine shafts or railway tracks by a sudden change of the loading direction. The crack will initiate due to the plastic strain occasioning from the cyclic stress, whereas the propagation steps of the cracks result from the tensile stress. Furthermore, the cause of local tensile stresses happens to be the fact that compressive loads may not lead to the initiation of fatigue crack [20]. To prevent failure due to fatigue, extensive research has been performed to get developed and

effective models to predict fatigue crack propagation and fatigue lifetime. Several experimental models have been proposed, but carrying out the experiment is generally expensive and time-consuming. Numerical simulation using the extended finite element approach is a suitable way to minimize the time and cost associated with experimental work. Under linear elastic fracture mechanics (LEFM) analysis, the SIFs are used to describe displacements and stresses around the crack front as well as the analysis of fatigue crack propagation. As the crack propagates larger, the SIF increases, until it reaches a critical range, where the assembly might start to deform by initiating fracture. As a result of the complex mode of applied loads, the geometry specification, mixed modes (I/II) are regularly the general types of loads dependent on ΔK_{eq} used in the fatigue life prediction [21–24]. The aim of this paper is to use the extended finite element method implemented by ANSYS APDL 19.2 to investigate the effect of the loading angle for the CTS specimen with different initial cracks.

2. Numerical Predication of Mixed-Mode Fatigue Life

Mainly, three approaches have been commonly used for illustration of the fatigue assessment of materials which are the fracture mechanics method established by [25], the strain-life method proposed independently by [26], and the stress-life method proposed by [27]. In the present study, the first method was used for fatigue life prediction by which the crack tip can be individually defined by the SIFs. Therefore, it is essential to estimate the fatigue crack path accurately in order to predict the fatigue life assessment. To this end, the maximum tangential stress criterion theory was used to predict the crack deflection angle [28–30] as

$$\theta = 2\arctan\left(\frac{1}{4}\frac{K_I}{K_{II}} + \frac{1}{4}\sqrt{\left(\frac{K_I}{K_{II}}\right)^2 + 8}\right), \quad \text{for } K_{II} < 0,$$
(1)

$$\theta = 2\arctan\left(\frac{1}{4}\frac{K_I}{K_{II}} - \frac{1}{4}\sqrt{\left(\frac{K_I}{K_{II}}\right)^2 + 8}\right), \quad \text{for } K_{II} > 0.$$
(2)

The two possibilities for the crack growth direction are shown in Figure 1.

The calculation of fatigue crack growth using the corresponding stress intensity factor is the most widely used method for structures under mixed-mode dynamic loading. Using a modified formula of Paris law, a researcher [24] proposed a power law for the fatigue crack growth relationship with ΔK_{eq}, which is specified as

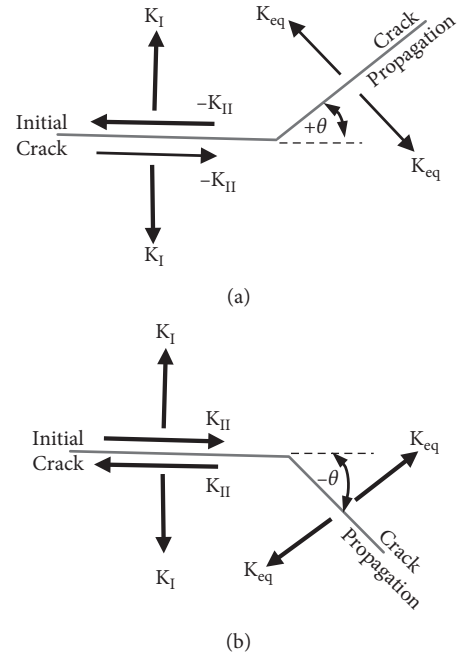$$\frac{da}{dN} = C\left(\Delta K_{eq}\right)^m$$
(3)

(a)

(b)

FIGURE 1: Crack growth angle. (a) $K_{II} > 0$, (b) $K_{II} < 0$.

From equation (3), for a crack increment, the number of life cycles of fatigue may be predicted as

$$\int_0^{\Delta a} \frac{da}{C\left(\Delta K_{eq}\right)^m} = \int_0^{\Delta N} dN = \Delta N.$$
(4)

Several of the commonly used ΔK_{eq} formulas accompanied by the proposed authors are listed in Table 1.

2.1. Numerical Results and Discussion. Finite element code ANSYS Mechanical APDL 19.2 is implemented to simulate the different types of loading angle of the compact tension specimen (CTS). The CTS geometry is shown in Figure 2(a) and its suggested loading angles are shown in Figure 2(b). There are three types of cracks that can be introduced in ANSYS which are arbitrary, semielliptical, and premeshed crack. The premeshed crack method involves the crack front that is used by the Smart Crack Growth analysis engine where the failure criterion is the stress intensity factor. The previously created node sets are allocated to the crack front within the premesh crack unit and the top and bottom faces of the crack. The crack coordinate system is referenced. The number of contours for solution is set to 5. These are the "loops" through the mesh around the crack tip, which are used to evaluate the stress intensity factor by integrating the crack tip region strain energy. In the analysis the fracture mechanics method avoids the stress singularities at the crack tip. The process is repeated for the top and bottom crack faces. The new implemented feature in ANSYS is the "Smart Crack Growth" with tetrahedron mesh added after finishing the requirements of the "premeshed crack," in which the user can select the type of crack growth option.

TABLE 1: Commonly applied ΔK_{eq} formulas.

Model provided by authors	ΔK_{eq} expression
[24]	$\Delta K_{eq} = (\Delta K_I^2 + 2\Delta K_{II}^2)^{1/2}$
[24]	$\Delta K_{eq} = (\Delta K_I^4 + 8\Delta K_{II}^4)^{1/4}$
[31]	$\Delta K_{eq} = \sqrt{\Delta K_1^2 + \Delta K_{II}^2}$
[32, 33]	$\Delta K_{eq} = \dfrac{\Delta K_I}{2} + \dfrac{1}{2}\sqrt{\Delta K_I^2 + 4(1.155\Delta K_{II}^2)}$
[21]	$\Delta K_{eq} = (1.0519 \times K_I^4 - 0.035 \times K_{II}^4 + 2.3056 \times K_I^2 \times K_{II}^2)^{1/2}$
[34]	$\Delta K_{eq} = \cos\dfrac{\theta}{2}[K_I\cos^2\dfrac{\theta}{2} - \dfrac{3}{2}K_{II}\sin\theta]$
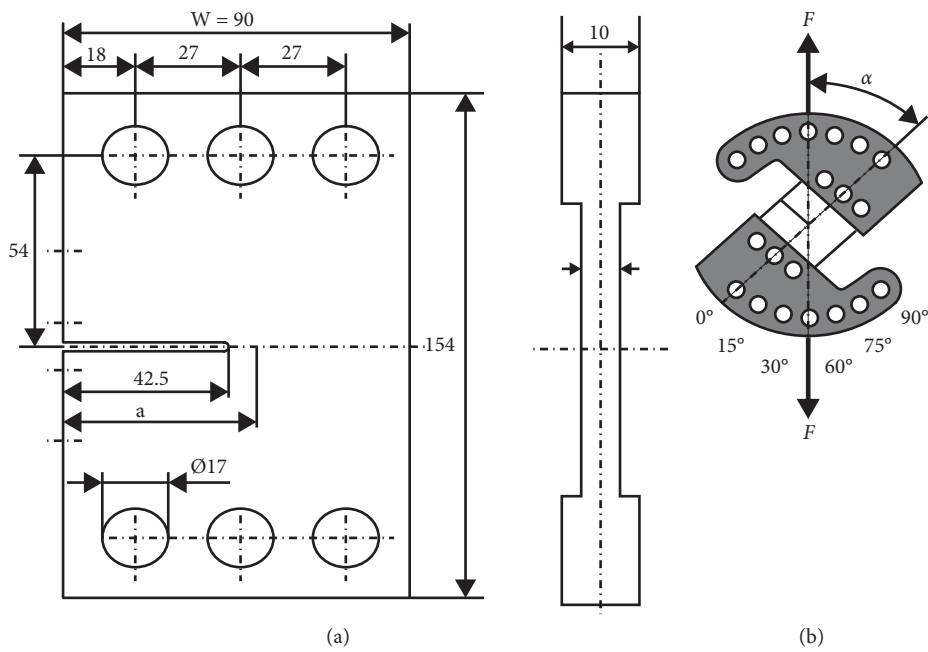
FIGURE 2: CTS geometry: (a) dimensions (in mm) and (b) loading angles.

FIGURE 3: 3D ANSYS model for CTS specimen (no. of nodes = 201317 and no. of elements = 132886).

Figure 3 displays the 3D finite element layout for the geometry dimensions of the CTS with number of nodes = 201317 and number of elements = 132886. Based on the values of the loading angle (α), which can be changed in stages of 15° from 0 to 90°, the modes of loading will change according to the value of the angle from mixed-mode loading ($\alpha = 15°$, 30°, 45°, 60°, and 75°), pure mode II ($\alpha = 0°$), and pure mode I ($\alpha = 90°$). The studied material was aluminium alloy having an elasticity module of $E = 74$ GPa, $v = 0.33$, $\sigma_Y = 517$ MPa, tensile strength = 579 MPa, fracture toughness $K_{IC} = 32.95$ MPa $\sqrt{m}$, threshold SIF $K_{th} = 3.15$ MPa $\sqrt{m}$, Paris constant $C = 4.3378 \times 10^{-7\ 7}$ (mm/cycle)/(MPa $\sqrt{m}$), and Paris exponent, $m = 2.6183$ [35].

The geometry's thickness is 5 mm while the ending parts' thicknesses are 10 mm, which can protect the specimen's linking holes from failing. The plane-stress conditions are assumed in the simulations according to the thickness value which is small compared to other dimensions as well as for precise comparison with other researchers who assumed that for the same geometry [35]. The value of load is $P = 16$ kN and the precrack length is $a = 45$ mm.

The finite element model of ANSYS shown in Figure 3 is completely consistent with the state of experimental tests performed by [21, 35–37]. In the present simulation, the CTS geometries are loaded in various angles 30°, 45°, 60°, and 75° in the original direction of cracking for the comparison of ΔK_{eq} and crack paths directions. There are also other loading angles 0°, 30°, 60°, and 90° to compare the direction of crack propagation and assessment of fatigue life. In the last case, three different crack length geometries of the CTS geometries have been simulated according to the initial crack length of $a/W = 0.3$, 0.5, and 0.7.

Figure 4 shows the distribution of the equivalent loading used in ANSYS analysis of the present work. The uniaxial load F is correlated to the equivalent loads acting on different holes of the six holes based on the following formulas [38]:

$$F_1 = F_6 = F\left(0.5 \cos \alpha + \frac{c}{b} \sin \alpha\right),$$

$$F_2 = F_5 = F \sin \alpha, \tag{5}$$

$$F_3 = F_4 = F\left(0.5^* \cos \alpha - (c/b)\sin \alpha\right).$$

where α is the angle of load and c and b are length parameter shown by Figure 4 ($c = b = 54$ mm). The final values of all loading forces with different loading angles are shown in Table 2.

The analytical solution for K_I of this specimen is provided by [23] as

$$K_I = \frac{F}{Wt} \sqrt{\pi a} \frac{\cos \alpha}{(1 - a/W)} \sqrt{\frac{0.26 + 2.65 \alpha/(W - a)}{1 + 0.55 \alpha/(W - 5) - 0.08 (a/(W - a))^2}}, \tag{6}$$

where F is the uniaxial load (Figure 2(b)), a is a crack's length, W is the width of geometry, and t is the geometry thickness. It is worth comparing the SIFs for this geometry with the analytical solution of K_I, (equation (6)), for different thicknesses (3, 6, 9, and 12 mm) as represented in Figure 5.
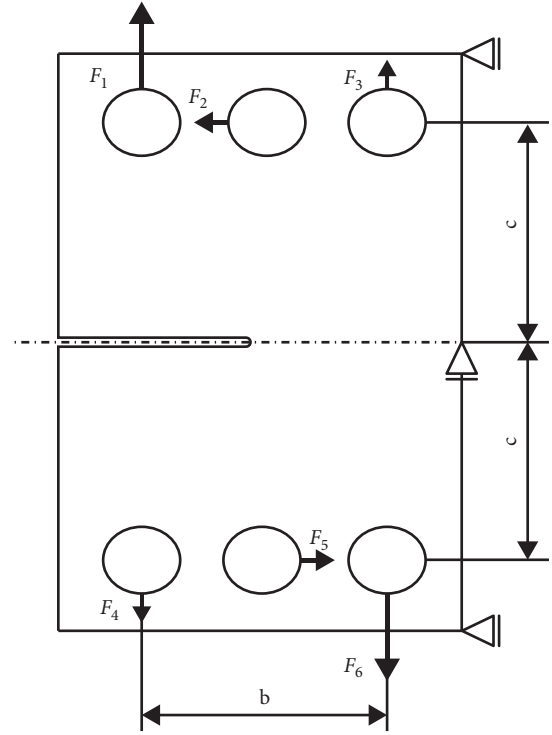

Figure 4: Loading and boundary condition for CTS geometry.

Table 2: Values of forces $F1$ to $F6$ according to load angle α

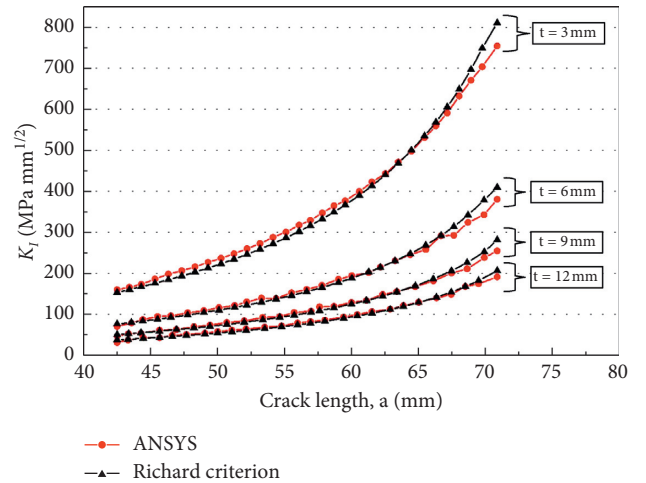| α	$F_2 = F_5$	$F_1 = F_6$	$F_3 = F_4$
15	0.259 F	0.742 F	0.224 F
30	0.5 F	0.933 F	−0.067 F
45	0.707 F	1.061 F	−0.354 F
60	0.866 F	1.116 F	−0.616 F
75	0.966 F	1.095 F	−0.837 F
90	F	F	−F

Figure 5: Comparison for K_I with analytical solution for different specimen thicknesses 3 mm, 6 mm, 9 mm, and 12 mm.
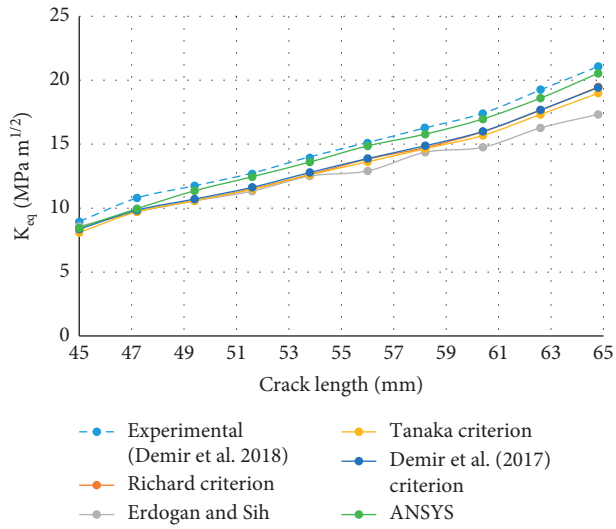
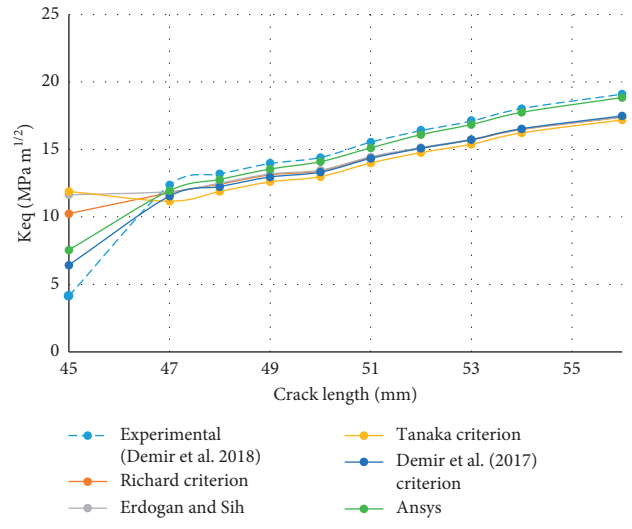Figure 6: Equivalent SIF with loading angle 30°.
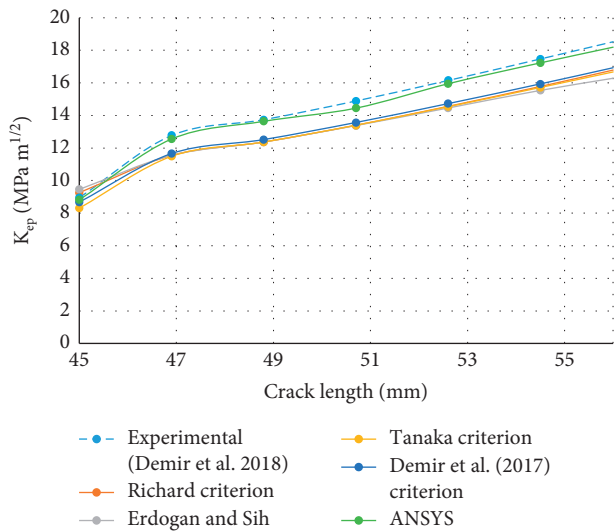

Figure 7: Equivalent SIF with loading angle 45°.

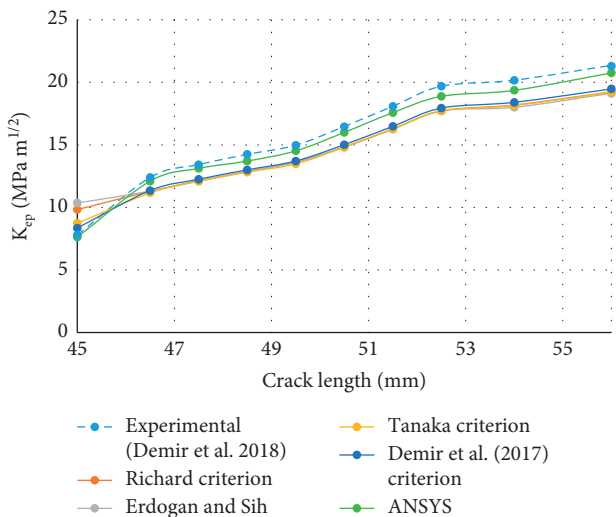Figure 8: Equivalent SIF with loading angle 60°.

Figure 9: Equivalent SIF with loading angle 75°.

As can be seen in this figure the values of SIFs are decreasing as the thickness increasing and the agreement with the analytical solution obtained by equation (2) is obvious.

The predicted values of ΔK_{eq} were compared to the experimental values performed by [37] as well as the analytical expression given by [24, 33, 34, 37] for different values of loading angles 30°, 45°, 60°, and 75°. These comparisons are shown in Figures 6–9.

Figure 6 demonstrates the comparisons for the variation of the crack length as a function of the corresponding ΔK_{eq} with load angle of 30° and the amount of applied loading is 8.8 kN (loading ratio $R = 0.1$). As illustrated in this figure, the four criteria of ΔK_{eq} have around the same tendency as data obtained from experimental tests by [37]. For this loading angle even there is a slight divergence for the [34] criterion especially after the mid of the crack length. In Figure 7, the loading angle is 45° and the amount of the load is 11.4 kN with $R = 0.1$. The agreement for the ANSYS results with the experimental results is clear as well as with other analytical criteria.

Figure 8 shows the comparisons for the equivalent SIF for 60° loading angle and the amount of load is 13.65 kN with load ratio $R = 0.1$. There is clearly divergence of the initial values of the equivalent SIF for all criteria which is dependent in the initial step of the crack growth. This divergence is increased for the loading angle of 75° and amount of load is 13 kN ($R = 0.1$) as shown in Figure 9. Though, all of the four criteria almost provide close predictions to the experimental results obtained by [37].

In addition, the paths of crack growth of load angles 30°, 45°, 60°, and 75° were validated with comparison to practical crack paths tested by [36] as shown in Figure 10 with good agreement.

The predicted crack growth path has been compared to the experimental test performed by [39] with different crack lengths ($a/w = 0.3$, 0.5, and 0.7) and different load angles 0, 30, 60, and 90 as shown in Table 3.

For pure loading of mode II ($\alpha = 0°$), the direction of the crack growth is controlled by the second mode of SIF (K_{II})
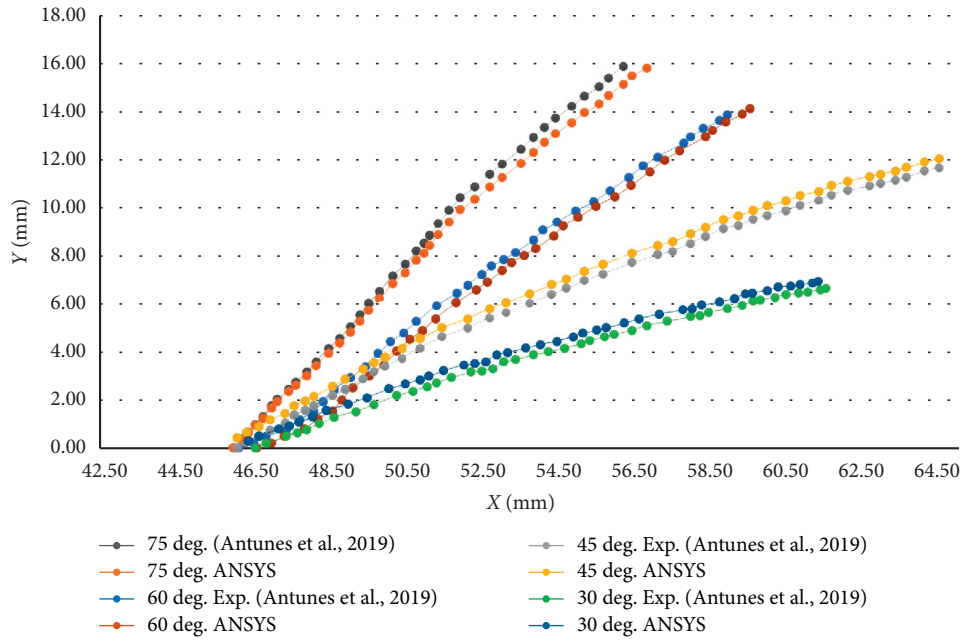
FIGURE 10: Comparison for crack growth paths between present study results and experimental results of [36].

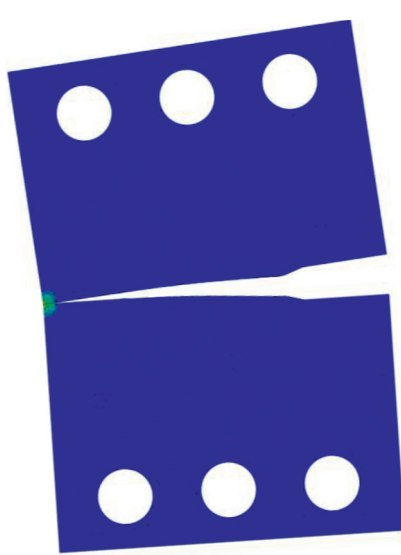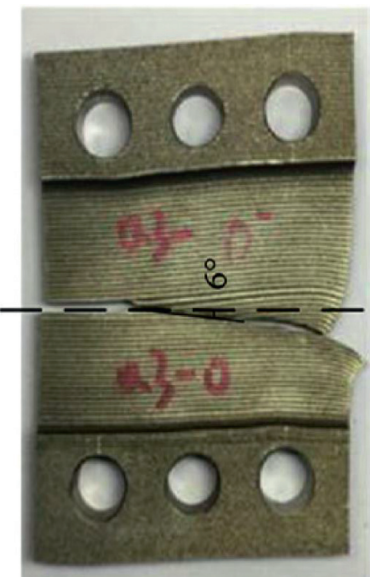TABLE 3: Comparison of paths of crack propagation among ANSYS's results and experimental results [39].

ANSYS	Experimental test [39]
(a/w = 0.3) $\alpha = 0°$	

Table 3: Continued.
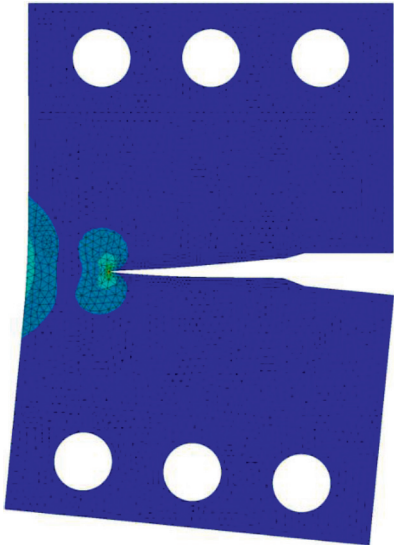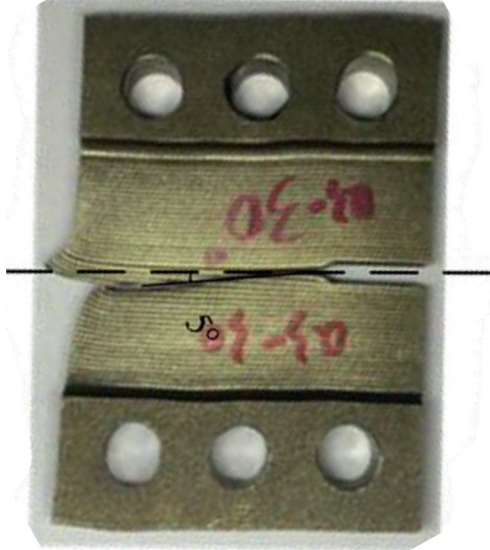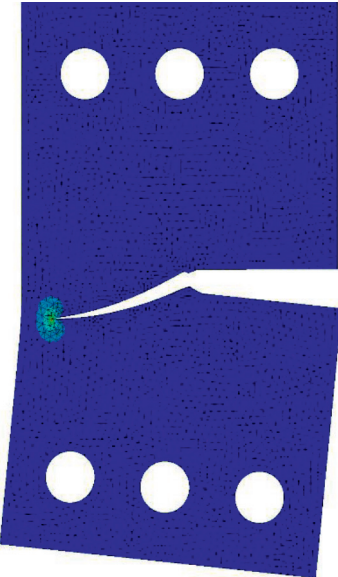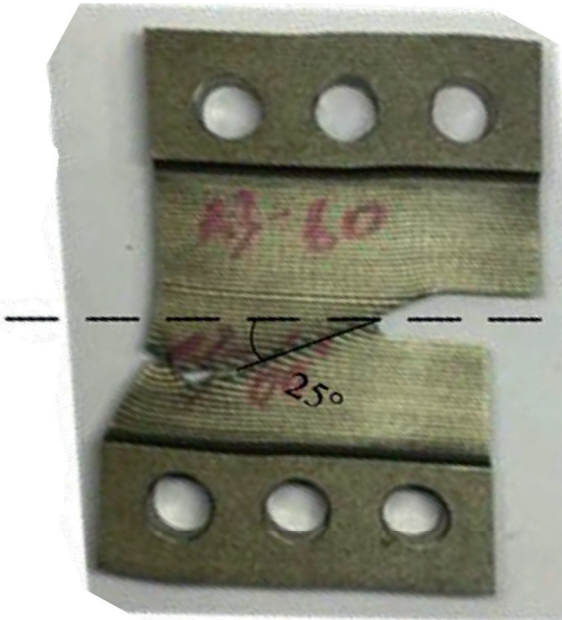
ANSYS	Experimental test [39]
$(a/w = 0.3)$ $\alpha = 30°$	
$(a/w = 0.3)$ $\alpha = 60°$	

TABLE 3: Continued.
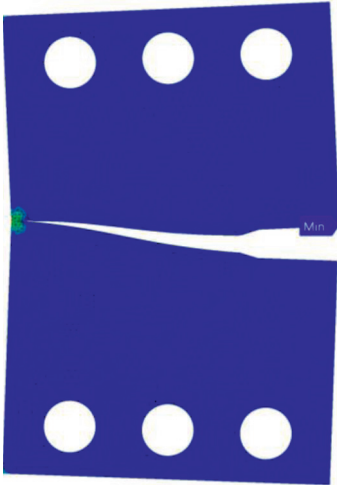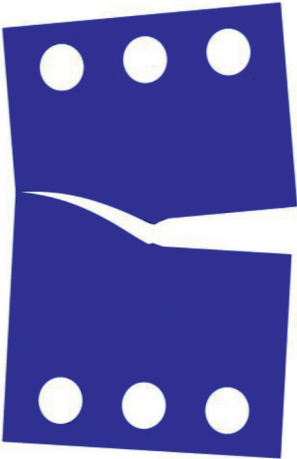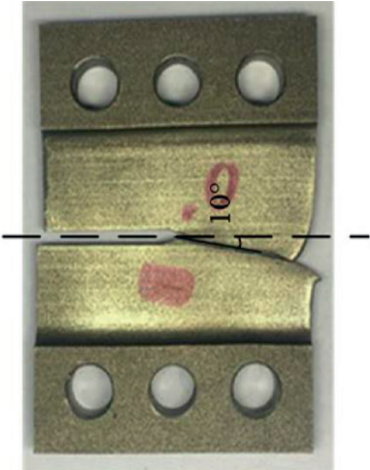
ANSYS	Experimental test [39]

(a/w = 0.3) $\alpha = 90°$

(a/w = 0.5) $\alpha = 0°$

Table 3: Continued.
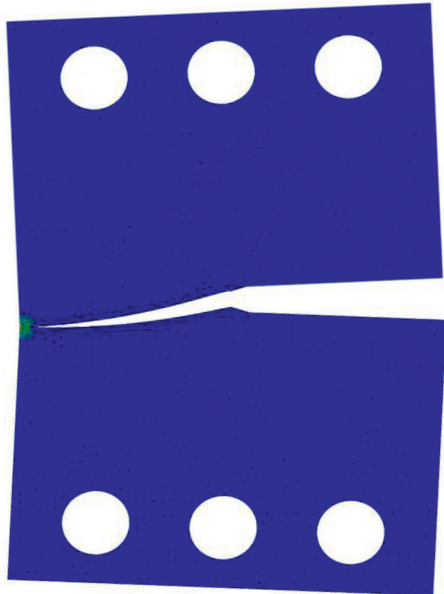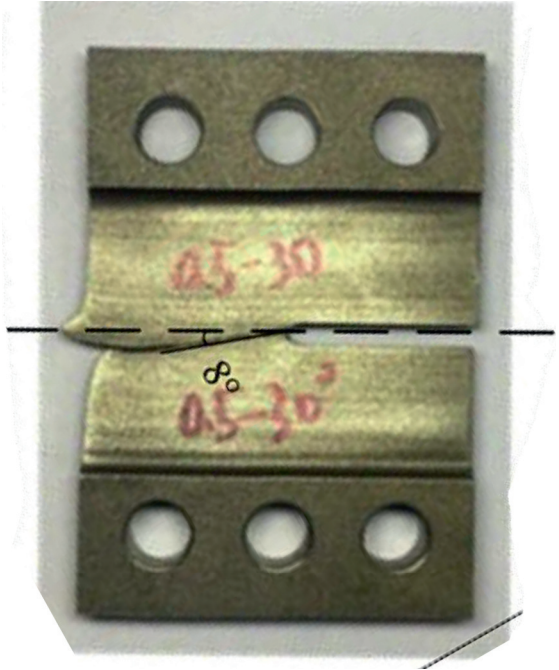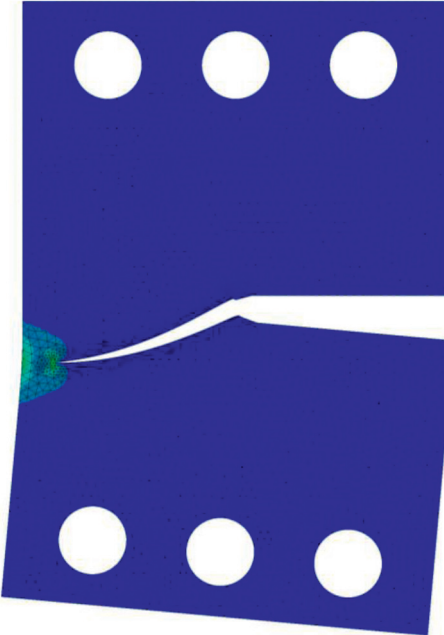
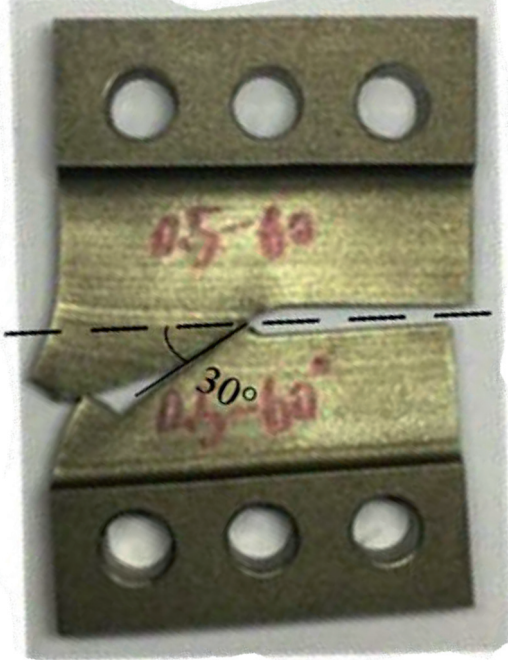| ANSYS	Experimental test [39]

(a/w = 0.5) $\alpha = 30°$

(a/w = 0.5) $\alpha = 60°$

TABLE 3: Continued.
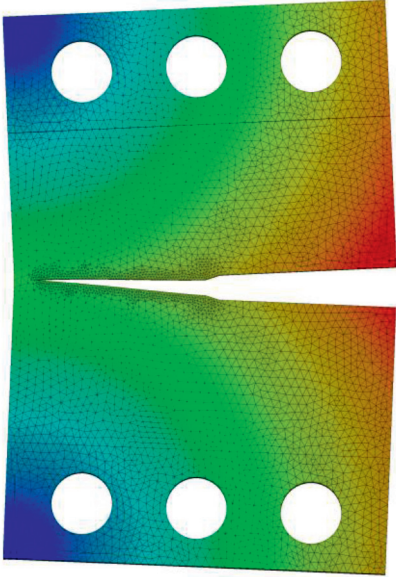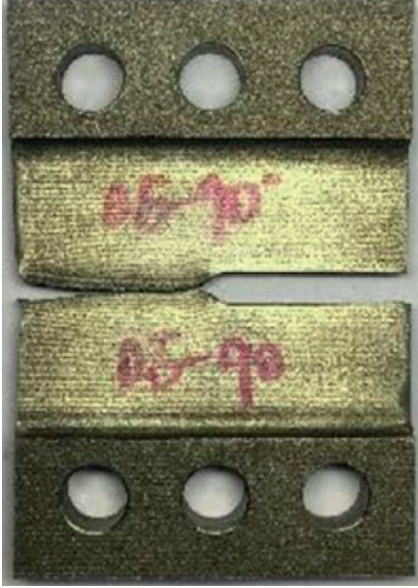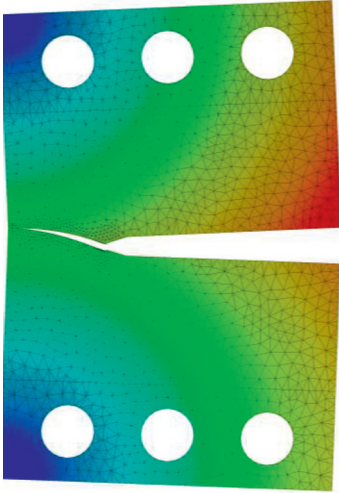
ANSYS	Experimental test [39]
(a/w = 0.5) $\alpha = 90°$	

| **(a/w = 0.7)** $\alpha = 0°$ | |

TABLE 3: Continued.
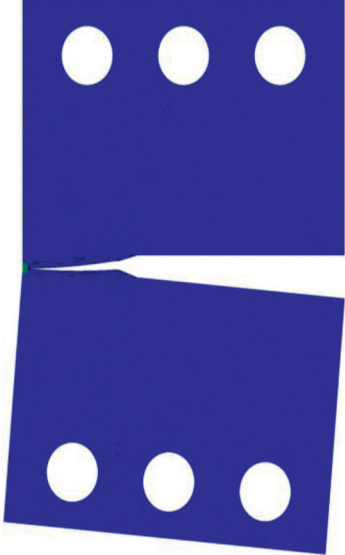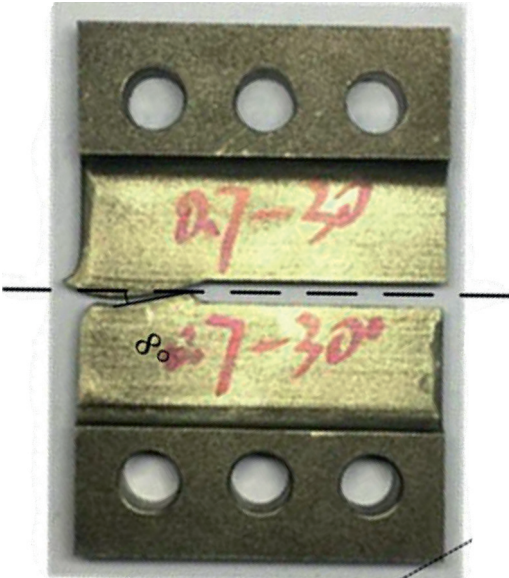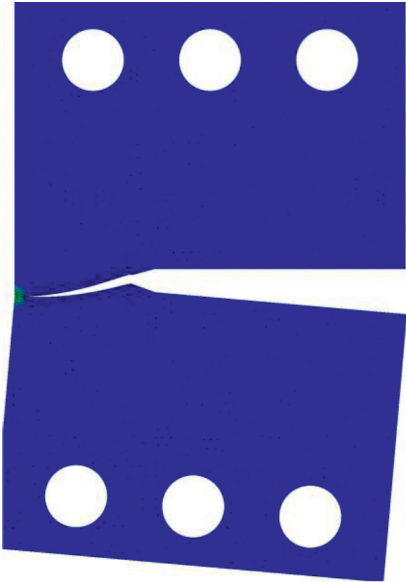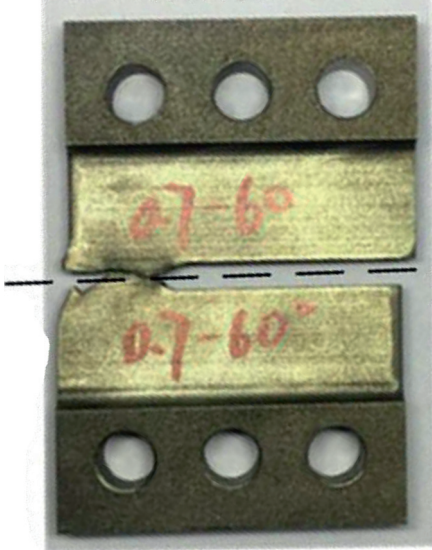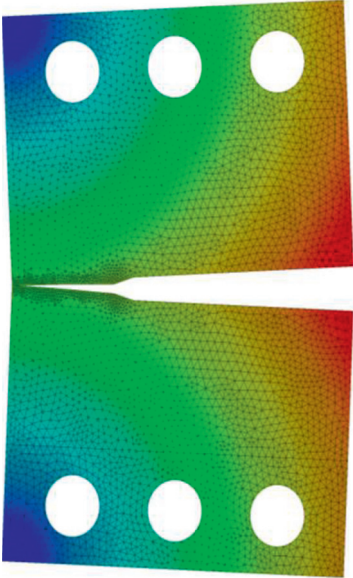
ANSYS	Experimental test [39]

$(a/w = 0.7)$ $\alpha = 30°$

$(a/w = 0.7)$ $\alpha = 60°$

ANSYS	Experimental test [39]
$(a/w = 0.7)$ $\alpha = 90°$	

FIGURE 11: Comparison of simulated and experimental [35] fatigue life for loading angle 30°.
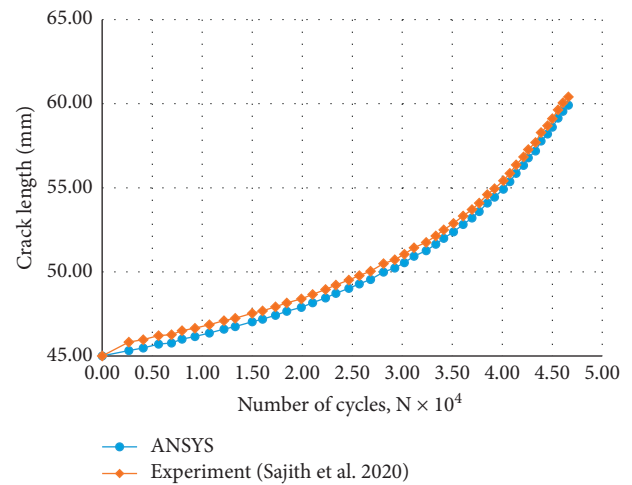
FIGURE 12: Comparison of simulated and experimental [35] fatigue life for loading angle 60°.

and the cracks all grow with different angles based on equation (2) as the values of K_{II} are higher, whereas for complete mode I loading ($\alpha = 90°$), crack paths are dominated by the first mode K_I and the crack is going to grow straight. The influence of the first mode (K_I) decreases as α increases and vice versa for mode II.

The crack direction angles of three geometries with different initial length of cracks ($a/W = 0.3$, 0.5, and 0.7) are 6°, 10°, and 12°, respectively, which are identical to the experimental angles tested by [39]. Furthermore, for mixed-mode loading in the CTS geometries with loading angle $\alpha = 30°$, the cracks are propagated to some extent differing to the original crack front direction. For these three geometries, the mixed-mode crack propagation angles ($a/W = 0.3$, 0.5, and 0.7) are about 5.5°, 8.5°, and 8.5°, respectively, which are almost in agreement with experimental angles of [39].

For the above three loading angles situations ($\alpha = 90°$, $\alpha = 0°$, and $\alpha = 30°$), regardless of the length of the initial crack for the same load angle (α), the angles of the crack growth in each case are close to each other. In contrast, for combined mode (I/II) loading with loading angle $\alpha = 60°$, the directions of crack are highly dependent on the initial length of the crack. On the other hand, for small crack length (a/W = 0.3 and 0.5), the cracks also grow varying from the initial crack tip against the clockwise direction, with crack propagation angles of 25° and 30°, respectively, which are identical to those angles in the experimental test [39]. Furthermore, if the initial crack length is longer than the previous cases (a/W = 0.7), the direction of the crack growth and the direction of the initial crack happen to be identical and are presented in Table 3.

In order to assess the fatigue life, the number of cycles for different loading angles 30 and 60 calculated in this study is compared with the experimental results observed by [35] under mixed loading mode (I/II) resulting in clear agreements as can be observed in Figures 11 and 12. The amount of the applied load is $F = 16$ kN with load ratio $R = 0.1$, whereas the Paris constant as mentioned previously is $C = 4.3378 \times 10^{-7}$ (mm/cycle)/(MPa $\sqrt{m}$) and $m = 2.6183$ [40].

3. Conclusions

For the CTS specimen, the finite element analysis of the mixed-mode fatigue crack propagation was carried out using ANSYS Mechanical APDL and compared with experimental data for various angles of loading. The predicted values of ΔK_{eq} by the experimental and numerical methods are observed to be in good agreement with the present study results. The mixed-mode fatigue life is predicted and compared with experimental data for two different loading angles of 30° and 60°. Interestingly, the theoretically predicted trajectories of the crack growth for all specimens are identical to the experimental determined paths for different loading angles. Furthermore, the predicted values of SIFs (K_I and K_{II}) are in good agreement with analytical solutions. It can be stated that the structure of specimen geometry and its configuration play an important role in obtaining higher values of mixed-mode SIFs values. This happens to be significant in terms of applied loads particularly for higher values of K_{II}.

Data Availability

The data used to support the findings of this study are included within the article.

Conflicts of Interest

The authors declare that they have no conflicts of interest.

References

[1] R. I. Stephens, A. Fatemi, R. R. Stephens, and H. O. Fuchs, *Metal Fatigue in Engineering*, John Wiley & Sons, Hoboken, NJ, USA, 2000.

[2] V. V. Bolotin, *Mechanics of Fatigue*, CRC Press, Boca Raton, FL, USA, 1999.

[3] C. A. Brebbia and A. V. Farahani, *Fatigue Damage of Materials: Experiment and Analysis*, WIT Press, Southampton, UK, 2003.

[4] N. E. Dowling, *Mechanical Behavior of Materials: Engineering Methods for Deformation, Fracture, and Fatigue*, Pearson, London, UK, 2012.

[5] G. R. Halford, *Fatigue and Durability of Structural Materials*, ASM International, London, UK, 2006.

[6] R. O. Ritchie, "Mechanisms of fatigue-crack propagation in ductile and brittle solids," *International Journal of Fracture*, vol. 100, no. 1, pp. 55–83, 1999.

[7] S. Suresh, *Fatigue of Materials*, Cambridge University Press, Cambridge, UK, 1998.

[8] K. N. Solanki, *Two and Three-Dimensional Finite Element Analysis of Plasticity-Induced Fatigue Crack Closure: A Comprehensive Parametric Study*, Mississippi State University, Starkville, MS, USA, 2002.

[9] A. M. Alshoaibi and A. K. Ariffin, "Finite element modeling of fatigue crack propagation using a self adaptive mesh strategy," *International Review of Aerospace Engineering (IREASE)*, vol. 8, no. 6, pp. 209–215, 2015.

[10] A. M. Alshoaibi, "Finite element procedures for the numerical simulation of fatigue crack propagation under mixed mode loading," *Structural Engineering and Mechanics*, vol. 35, no. 3, pp. 283–299, 2010.

[11] A. M. Alshoaibi, "Adaptive finite element modeling of fatigue crack propagation," *International Journal of Materials Science and Applications*, vol. 2, no. 3, pp. 104–108, 2013.

[12] A. M. Alshoaibi, "An adaptive finite element framework for fatigue crack propagation under constant amplitude loading," *International Journal of Applied Science and Engineering*, vol. 13, no. 3, pp. 261–270, 2015.

[13] A. M. Alshoaibi, "Comprehensive comparisons of two and three dimensional numerical estimation of stress intensity factors and crack propagation in linear elastic analysis," *International Journal of Integrated Engineering*, vol. 11, no. 6, pp. 45–52, 2019.

[14] A. Handbook, *Fatigue and Fracture American Society of Materials*, vol. 19, 1996.

[15] W. He, J. Liu, and D. Xie, "Numerical study on fatigue crack growth at a web-stiffener of ship structural details by an objected-oriented approach in conjunction with ABAQUS," *Marine Structures*, vol. 35, pp. 45–69, 2014.

[16] K. Rege and D. G. Pavlou, "Effect of stop holes on structural integrity of offshore structures: a numerical model," in *Proceedings of the Institution of Civil Engineers-Maritime Engineering*, Thomas Telford Ltd, London, UK, 2019.

[17] H. Rhee, "Fatigue crack growth analyses of offshore structural tubular joint," *Journal of Offshore Mechanics and Arctic Engineering*, vol. 111, no. 1, pp. 49–55, 1989.

[18] H. Riahi, P. Bressolette, A. Chateauneuf, C. Bouraoui, and R. Fathallah, "Reliability analysis and inspection updating by stochastic response surface of fatigue cracks in mixed mode," *Engineering Structures*, vol. 33, no. 12, pp. 3392–3401, 2011.

[19] S. Qi, L. X. Cai, C. Bao, H. Chen, K. K. Shi, and H. L. Wu, "Analytical theory for fatigue crack propagation rates of mixed-mode I-II cracks and its application," *International Journal of Fatigue*, vol. 119, pp. 150–159, 2019.

[20] A. F. Liu, *Mechanics and Mechanisms of Fracture: An Introduction*, ASM International, London, UK, 2005.

[21] O. Demir, A. O. Ayhan, and S. İriç, "A new specimen for mixed mode-I/II fracture tests: modeling, experiments and

criteria development," *Engineering Fracture Mechanics*, vol. 178, pp. 457–476, 2017.

[22] M. Hussain, S. Pu, and J. Underwood, "Strain energy release rate for a crack under combined mode I and mode II. Fracture Analysis," in *Proceedings of the 1973 National Symposium on Fracture Mechanics, Part II*, ASTM International, West Conshohocken, PA, USA, 1974.

[23] H. Richard, M. Sander, M. Fulland, and G. Kullmer, "Development of fatigue crack growth in real structures," *Engineering Fracture Mechanics*, vol. 75, no. 3-4, pp. 331–340, 2008.

[24] K. Tanaka, "Fatigue crack propagation from a crack inclined to the cyclic tensile axis," *Engineering Fracture Mechanics*, vol. 6, no. 3, pp. 493–507, 1974.

[25] P. Paris and F. Erdogan, "A critical analysis of crack propagation laws," *Journal of Basic Engineering*, vol. 85, no. 4, pp. 528–533, 1963.

[26] L. Coffin, "Cyclic deformation and fatigue of metals," *The Book, Fatigue and Staying Power of Metals*, Izo. IL, USSR, Moscow, Russia, 1963.

[27] A. Wöhler, "Versuche zur Ermittlung der auf die Eisenbahnwagenachsen einwirkenden Kräfte und die Widerstandsfähigkeit der Wagen-Achsen," *Zeitschrift für Bauwesen*, vol. 10, no. 1860, pp. 583–614, 1860.

[28] J. M. Alegre, M. Preciado, and D. Ferreño, "Study of the fatigue failure of an anti-return valve of a high pressure machine," *Engineering Failure Analysis*, vol. 14, no. 2, pp. 408–416, 2007.

[29] H. Chen, Q. Wang, W. Zeng et al., "Dynamic brittle crack propagation modeling using singular edge-based smoothed finite element method with local mesh rezoning," *European Journal of Mechanics—A/Solids*, vol. 76, pp. 208–223, 2019.

[30] S. Sajith, K. S. R. Krishna Murthy, and P. Robi, "Prediction of Accurate Mixed Mode Fatigue Crack Growth Curves using the Paris' Law," *Journal of The Institution of Engineers (India): Series C*, vol. 100, no. 1, pp. 165–174, 2019.

[31] G. R. Irwin, "Analysis of stresses and strains near the end of a crack transversing a plate," *Journal of Applied Mechanics*, vol. 24, pp. 361–364, 1957.

[32] H. A. Richard, F. G. Buchholz, G. Kullmer, and M. Schöllmann, *2D-and 3D-mixed mode fracture criteria. Key Engineering Materials*, Trans Tech Publication, Stafa-Zurich, Switzerland, 2003.

[33] H. A. Richard, B. Schramm, and N.-H. Schirmeisen, "Cracks on Mixed Mode loading - Theories, experiments, simulations," *International Journal of Fatigue*, vol. 62, pp. 93–103, 2014.

[34] F. Erdogan and G. C. Sih, "On the crack extension in plates under plane loading and transverse shear," *Journal of Basic Engineering*, vol. 85, no. 4, pp. 519–525, 1963.

[35] S. Sajith, K. S. R. K. Murthy, and P. S. Robi, "Experimental and numerical investigation of mixed mode fatigue crack growth models in aluminum 6061-T6," *International Journal of Fatigue*, vol. 130, p. 105285, 2020.

[36] F. Antunes, R. Branco, J. Ferreira, and L. Borrego, "Stress intensity factor solutions for CTS mixed mode specimen," *Frattura ed Integrità Strutturale*, vol. 13, no. 48, pp. 676–692, 2019.

[37] O. Demir, A. O. Ayhan, S. Iric, and H. Lekesiz, "Evaluation of mixed mode-I/II criteria for fatigue crack propagation using experiments and modeling," *Chinese Journal of Aeronautics*, vol. 31, no. 7, pp. 1525–1534, 2018.

[38] H. Richard, *Fracture predictions for cracks exposed to superimposed normal and shear stresses*, International Nuclear Information System, Vienna, Austria, 1985.

[39] X.-T. Miao, Q. Yu, C.-Y. Zhou, J. Li, Y.-Z. Wang, and X.-H. He, "Experimental and numerical investigation on fracture behavior of CTS specimen under I-II mixed mode loading," *European Journal of Mechanics—A/Solids*, vol. 72, pp. 235–244, 2018.

[40] S. Sajith, S. S. Shukla, K. S. R. K. Murthy, and P. S. Robi, "Mixed mode fatigue crack growth studies in AISI 316 stainless steel," *European Journal of Mechanics—A/Solids*, vol. 80, p. 103898, 2020.